Journal of The Electrochemical Society, **161** (3) C107-C114 (2014)
0013-4651/2014/161(3)/C107/8/$31.00 © The Electrochemical Society

Nanometer-Scale Corrosion of Copper in De-Aerated Deionized Water

Christopher Cleveland,[a] Saeed Moghaddam,[b] and Mark E. Orazem[a,*,z]

[a]*Department of Chemical Engineering, University of Florida, Gainesville, Florida 32611, USA*
[b]*Department of Mechanical and Aerospace Engineering, University of Florida, Gainesville, Florida 32611, USA*

Copper is commonly regarded to be immune to corrosion in deaerated deionized electrolytes. The present work shows that, in the absence of hydrogen, copper will corrode on the order of 1 nm/day in deionized water with an O_2 concentration on the order of, or less than, 1 ppb. While a corrosion rate of this magnitude can normally be neglected, it may be catastrophic for nanoscale copper structures utilized in emerging applications to enhance energy transport at the solid-electrolyte interface, such as in cooling advance electronics. This conclusion is supported by a set of experimental and analytical studies that encompass impedance spectroscopy, slow-scan linear sweep voltammetry, thermodynamic calculations for the environment under study, and kinetic simulations. The studies provide a comprehensive insight on details of the corrosion mechanism for copper in deaerated water.
 [DOI: 10.1149/2.030403jes]

Manuscript submitted September 20, 2013; revised manuscript received December 9, 2013. Published December 31, 2013. This was Paper 1037 presented at the Toronto, ON, Canada, Meeting of the Society, May 12–16, 2013.

The need for increasingly more-functional electronics and the industry's ability to fabricate high density integrated circuits have led to an ever-increasing generation of waste heat in advanced electronics systems. The increases in heat generation has often been handled by improvements in materials or components configuration. However, it is now generally acknowledged that the cooling requirements for advanced electronics exceed the heat-removal capability of conventional cooling techniques. Liquid-based cooling[1-7] may remedy thermal management issues that have plagued development and deployment of enhanced electronic systems.

Due to its exceptional heat transfer characteristics, particularly in the phase change process, water is considered to be a suitable cooling fluid, so long as issues related to its electrical properties can be addressed. Numerous studies have been conducted to develop high performance water heat sinks.[8-13] These studies often utilize micro- or nanostructures to enhance heat transfer at the solid-liquid interface. Traditionally, copper has been the material of choice in water heat exchangers, and, as it is generally understood that copper does not corrode in deaerated deionized water, copper micro/nanostructures are implemented to benefit from the associated enhanced heat transfer characteristics.

The performance of micro/nanoscale copper structures has, however, been observed to degrade with time. Ju et al.[14] reported that corrosion in copper microfluidic channels used in a two-phase cooling system caused performance degradation. Since the cooling performance is intricately related to functionality of the liquid-vapor interface and fluid flow through a structure,[15] even small rates of corrosion can impair performance of a micro/nanostructured interface. Thus, an ability to predict and mitigate copper corrosion is needed.

The corrosion of copper in aerated media is relatively well understood. In acidic chloride solutions, for example, the corrosion of copper takes place by a mechanism that involves formation of $CuCl_2^{-1}$ from a CuCl intermediate.[16] The reaction process is reported to be diffusion controlled with no evidence of a protective oxide layer.[17] This mechanism has been presented as valid for temperatures as high as 165°C.[18]

A similar body of work does not exist for corrosion of copper micro/nanoscale structures in heat exchangers, though this area may be closely related to the body of work associated with plans for encasing nuclear waste in copper cladding. The standard equilibrium potential for the copper dissolution reaction has a value of 0.337 V with reference to the hydrogen reaction;[19] therefore, copper is commonly believed to be immune to corrosion in neutral deionized deaerated media. The proposed stability of copper in deaerated environments has motivated investigation of the feasibility for underground storage of nuclear waste in copper-lined containers.[20-26] Concern has been expressed over results presented by Hultquist[27] who showed that copper foil, stored for 15 years in a Erlenmeyer flask filled with deaerated deionized water and capped with a permeable membrane, selectively permitting the egress of hydrogen, revealed significant corrosion. Corrosion was not observed for a similar foil enclosed in a hermetically sealed flask that did not allow the effusion of hydrogen (or any gas). In a critique, King and Lilja identify some inconsistencies and indicate that other groups have been unable to reproduce Hultquist's results. Macdonald and Sharifi-Asl state, however, that Hultquist's results are not at odds with thermodynamics, provided that the concentration of Cu^+ and the partial pressure of hydrogen are suitably low.[25]

Bojinov et al. provided a mechanistic study of copper interactions with a deoxygenated neutral aqueous borate buffer solution.[28] Their preliminary conclusions were that no sustained corrosion of copper was found, but that the impedance results were consistent with an adsorbed CuOH intermediate associated with reduction of Cu(II) species. In an earlier study, Bojinov et al. used an on-line resistance probe to discover that copper corroded at an appreciable rate of 16 μm/y during short-time exposure to 1 M NaCl that contained very small amounts of oxygen.[29] After longer exposure, the corrosion rate decreased and back-deposition of copper was reported. As part of the analysis of the suitability of copper for nuclear waste storage, Sharifi-Asla and Macdonald[30] have performed studies of the hydrogen evolution reaction on copper in deoxygenated neutral aqueous borate buffer solutions.

Incidence of copper corrosion in deaerated deionized water has also been reported in the heat exchangers used to cool the synchrotron at Argonne National Labs. A study of corrosion rates as a function of oxygen content in neutral deionized water revealed that the corrosion rate was greater than 8 mg/m^2/day (0.9 nm/day), even at dissolved oxygen concentrations as low as 15 ppb.[31,32] These results were confirmed by subsequent analysis based on a non-stationary finite-difference simulation used to represent the processes of corrosion, erosion, dissolution, precipitation and deposition for the length of a 1-D cooling circuit. In this work, Parro found a corrosion rate of 1 g/m^2/year (0.3 nm/day).[33] These corrosion rates were considered to be sufficiently small as to pose no long-term problems with the operation of the synchrotron.

Small rates of corrosion may, however, be significant for heat exchangers in which surface nano-structure posts are utilized to fundamentally change the physics of liquid-surface interactions and to greatly enhance the phase-change heat transfer process. Small rates of corrosion may also compromise safe storage of nuclear waste where structural integrity must be assured for periods exceeding one million years.

*Electrochemical Society Fellow.
zE-mail: meo@che.ufl.edu

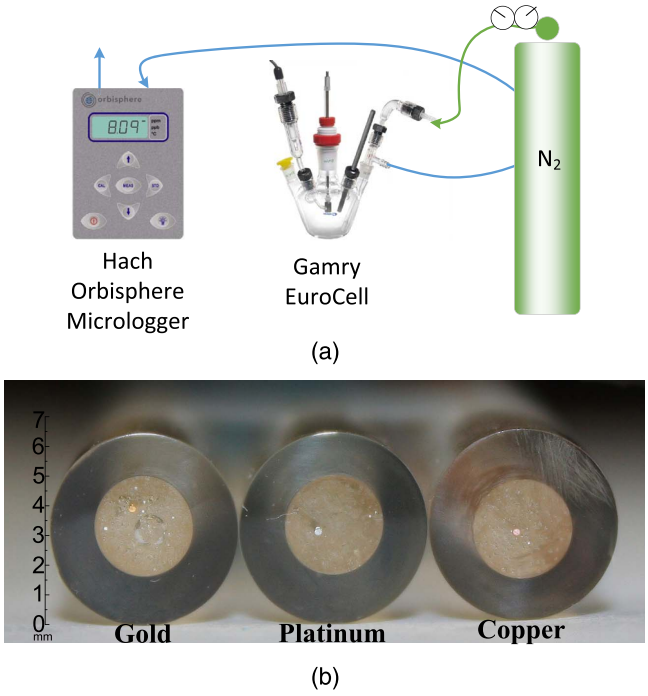

Figure 1. The electrochemical system: a) schematic diagram showing the deaeration process used to achieve 1-2 ppb gas-phase O_2 concentration levels, resulting in a substantially lower concentration in the water; and b) Cu, Au and Pt working electrodes with the exposed 0.25 mm disk diameter shown. The outside diameter of the plexiglas tube was 6.5 mm.

The objective of this work is to use electrochemical techniques to quantify corrosion of copper in pure deaerated water. The experimental techniques employed in this study include impedance spectroscopy and linear sweep voltametry. From these measurements, corrosion rates were determined and further validated with the use of kinetic modeling, and thermodynamic simulations.

Experimental

The experimental protocol, instrumentation, and electrodes are presented in this section.

De-Aeration procedure.— A five port 200 mL glass vessel (Gamry EuroCell), shown in Figure 1(a), was used as the electrochemical cell. The volume of electrolyte was 30 cm^3. The deionized water (Barnstead E-Pure D4631) had a resistivity of 17.6 MΩcm. BIP grade nitrogen gas (Airgas), with guaranteed 99.9999% purity was used to deaerate the system through a microporous glass frit for at least 1.5 h. A Hach Orbisphere 3650 micrologger, with a sensitivity of 0.1 ppb O_2, was used to monitor the O_2 concentration of the gas emanating from the cell, continuously until a stable 1-2 ppb gas-phase oxygen level was achieved. Under these conditions, the large Henry's Law constant for oxygen in water ensured that the oxygen level in the electrolyte was lower than 1 ppb.

To ensure that measurement of gas-phase O_2 concentration reflected the concentrations in the liquid phase, an experiment was devised in which the water from the electrochemical cell was conveyed under pressure to the oxygen detector. The water was de-aerated as discussed above until a stable 1-2 ppb gas-phase oxygen level was achieved. Pressure from the nitrogen tank was used to force the water from the vessel to the detector through Tygothane tubing (Saint-Gobain). Oxygen readings were taken after the 30 minute equilibration period recommended by the manufacturer for liquids having ppb levels of dissolved O_2. This measurement was repeated four times and the measured oxygen levels ranged from 8 ppb to 18 ppb. These values represent an upper limit to the oxygen content achieved in the electrolyte as the process introduced the potential ingress of small amounts of atmospheric oxygen. Indeed, the impedance response shown in a subsequent section indicates that the oxygen concentration in the water must have been less than 6.5 ppb.

Instrumentation.— Electrochemical experiments were performed for a three-electrode configuration using either a Gamry Reference 3000 or a Gamry Reference 600 potentiostat. For impedance measurements, open circuit potential (OCP) measurements were recorded until the OCP changed less than 0.1 mV/min. A grounded home-built Faraday cage was used to reduce electromagnetic interference. Impedance measurements were performed from 100 kHz to 200 mHz for experiments that explored the high-frequency dielectric response reported in a subsequent section. For studies of electrochemical reactivity, measurements were performed from 1 kHz to 50 mHz. The perturbation amplitude was 10 mV.

Linear sweep voltammetry was performed with a Gamry Reference 3000 using a sweep rate of 0.06 mV/s. Sweeps were performed from the open circuit potential in both anodic and cathodic directions. The working electrode for this experiment was a 0.1 mm diameter annealed 99.9% copper. The reference electrode and counter electrode were Ag/AgCl as reported below.

Electrodes.— The counter and reference electrodes were solid AgCl pellets embedded in a Plexiglas tube, sealed with epoxy, and attached to a silver wire. Two hours prior to impedance measurements, the Ag/AgCl electrodes were immersed in pure deionized water (with a resistivity of 17.6 MΩcm) and shorted together to reduce polarizing effects. The Ag/AgCl electrodes were used in this application to avoid electrochemical reactions that would change the electrolyte pH. The use of solid electrodes prevented contamination of the electrolyte by filling solutions used in conventional reference electrodes.

The working electrodes were composed of annealed 99.9% copper, hard-tempered 99.99+% gold, and annealed 99.9+% platinum (Goodfellow, UK) wires with 0.25 mm and 0.1 mm diameters. The wires were embedded in an epoxy mold to expose only a disk cross-section, as shown in Figure 1(b). Electrode surfaces were polished mechanically with the final polish performed using an alumina suspension with a 0.1 μm particle size until a fine mirror finish was visible. A series of organic solvents in increasing polarity (methanol, isopropanol, and acetone) followed by deionized water were used to clean and degrease the surface.

The impedance response for electrodes of diameter exceeding 0.5 mm was dominated by a high-frequency loop that, as discussed in a subsequent section, was attributed to the dielectric response of water. The 0.25 mm diameter electrodes were used in the present work to minimize the portion of the measured frequency range associated with the high-frequency loop, and thereby maximize the response associated with charging and faradaic currents at the electrode.

Experimental Results

The electrochemical measurements included impedance spectroscopy and linear sweep voltammetry. Impedance measurements on copper electrodes were repeated with inert gold and platinum electrodes in order to reveal differences in electrochemical behavior.

Impedance spectra.— Scaled impedance results, measured at the open-circuit condition, are presented in Figure 2 with electrode material as a parameter. The data shown were collected on a frequency range of 100 kHz to 200 mHz. The data were scaled by the apparent Ohmic resistance, obtained at the intersection between the high-frequency and the low-frequency loops, to emphasize the similarity in the high-frequency response for copper, gold, and platinum electrodes. As this feature is unaffected by the electrode material, it can be attributed to the dielectric response of water.

The values of the ohmic resistance obtained from the impedance response were 15.0 kΩcm^2 for the copper electrode, 19.5 kΩcm^2 for the gold electrode, and 12.8 kΩcm^2 for the platinum electrode. Slight

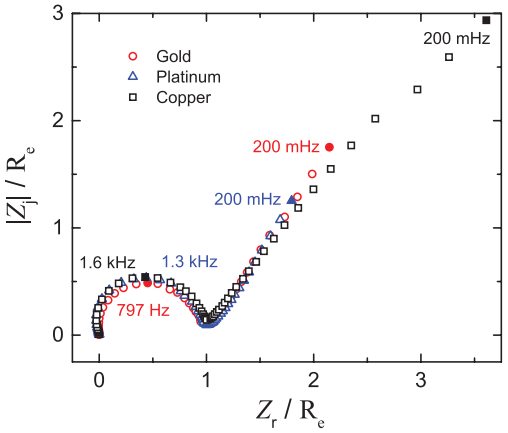

Figure 2. Scaled impedance response of copper, gold and platinum 0.25mm diameter electrodes in deaerated deionized water. The frequency range was 100 kHz to 40 mHz.

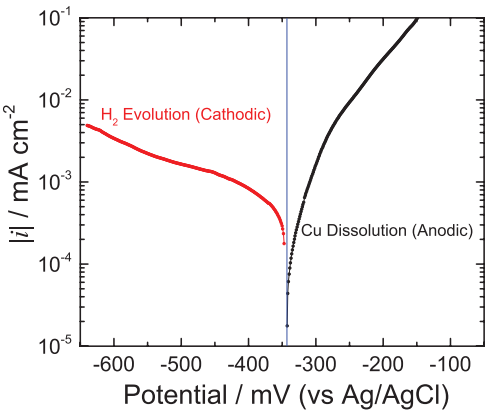

Figure 4. Polarization curve for copper deaerated with N_2 and obtained using a sweep rate of 0.06 mV/s from the open circuit potential in both anodic and cathodic directions.

differences in these values can be attributed to minute leaching of ions from the glassware. Following the formula for the ohmic resistance of a disk electrode presented by Newman,[34]

$$R_e = \frac{\rho}{4r_0} \quad [1]$$

the water resistivity for copper, gold, and platinum tests was calculated to be 1.53, 1.98, and 1.30 MΩcm, respectively. This estimated water resistivity is an order of magnitude lower than the initial 17.6 MΩcm water resistivity. A decrease in water resistivity is expected for experiments in highly deionized water.

A second set of experiments, which emphasize the low-frequency behavior, are presented in Figure 3. The frequency range, chosen to eliminate the influence of the high-frequency dielectric loop, is 54.5 Hz to 46.5 mHz. The Nyquist representation, shown in Figure 3(a), indicates that the gold and platinum electrodes had lower electrochemical reactivity than the copper electrode. The imaginary impedance is presented on logarithmic scale as a function of frequency in Figure 3(b). The slope of the imaginary impedance with respect to frequency indicates that the impedance data for the gold and platinum electrodes may be represented by a constant-phase-element model; whereas, the copper data indicates the presence of two time constants. As both anodic and cathodic electrochemical reactions are required to have an impedance response at open circuit, the impedance data presented for copper in Figure 3 suggest that corrosion may be taking place.

Polarization curves.— Polarization curves resulting from linear sweep voltammetry experiments are presented in Figure 4 for a copper electrode. The results were obtained using a sweep rate of 0.06 mV/s from the open circuit potential in both anodic and cathodic directions. The polarization curve in the anodic direction indicates the presence of corrosion, and the absence of a passivation plateau suggests the absence of oxide films. The composition and resistivity of the electrolyte changed in response to the electrochemical reactions. IR compensation could therefore not be performed, and a reliable Tafel slope could not be identified, precluding use of the polarization curve for accurate identification of the corrosion current. The polarization curve in the cathodic direction included reduction of species resulting from the anodic reaction at the Ag/AgCl counter electrode. The measurement of polarization curves caused changes in electrolyte composition that, while small, caused significant changes in the properties of the deionized water. The modifications to electrolyte properties were avoided in the impedance measurements by using a small perturbation amplitude at open circuit.

Simulations

The observation of corrosion is supported by a series of numerical simulations, including calculation of associated Pourbaix diagrams,

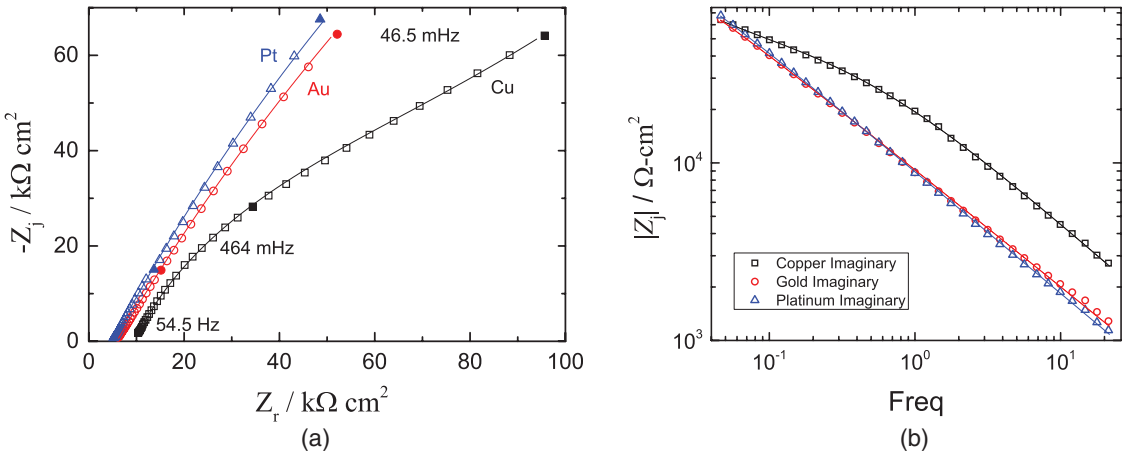

Figure 3. Low frequency impedance response of copper, gold and platinum 0.25mm diameter electrodes measured from 40 mHz to 100 kHz (Cu and Au) and from 200 mHz to 100 kHz (Pt): a) Nyquist Plot, and b) imaginary impedance as a function of frequency. The lines correspond to regression results corresponding to the models shown in Figure 7.

Table I. Liquid, vapor, and solid species considered in the thermodynamic analysis presented as Figure 5.

Aqueous Species	Vapor Species	Solid Species
H_2O	H_2O	Cu
Cu^+	H_2	Cu_2O
$Cu(OH)_2$	HNO_3	$Cu(OH)_2$
Cu^{+2}	O_2	$Cu(NO_3)_2 \cdot \frac{5}{2}H_2O$
$Cu(OH)^+$		$Cu(NO_3)_2 \cdot 6H_2O$
$Cu(NO_3)^+$		CuO
$Cu(NO_3)_2$		NaOH
$Cu(OH)_4^{-2}$		$NaOH \cdot H_2O$
$Cu(OH)_3^{-1}$		$NaNO_3$
H_2		$Cu(NO_3)_2$
H^+		Cu(OH)
OH^-		
NO_3^-		
HNO_3		
O_2		
Na^+		
$NaNO_3$		
Na(OH)		
$Na(OH) \cdot H_2O$		

kinetic simulation accounting for potential reactions, and regression analysis of the impedance results.

Thermodynamic analysis.— The possibility for corrosion under the conditions tested was explored by calculation of Pourbaix diagrams, presented in Figure 5, for pure copper in deaerated deionized water at 25°C. The titrants were assumed to be NaOH and HNO_3. The diagrams were generated by CorrosionAnalyzer 2.0 (Build 2.0.16) by OLI Systems Inc. The computational approach is described in greater detail by Anderko and co-workers.[35,36] The species considered in the thermodynamic analysis are presented in Table I.

The Pourbaix diagrams presented in Figure 5 are in good agreement with the Pourbaix diagrams presented by Beverskog and Puigdomenech for copper at 25°C.[37] The solid color marked Cu(s) represents the region in which copper is stable. The lines marked a and b are the equilibrium lines for evolution of hydrogen and oxygen, respectively, and the region between a and b can be described as the stability region for water. The natural pH, at which no titrants are added, is equal to 7. The redox potential for water, shown in Figure 5 by the lower filled circle at pH = 7, is on the equilibrium line a for

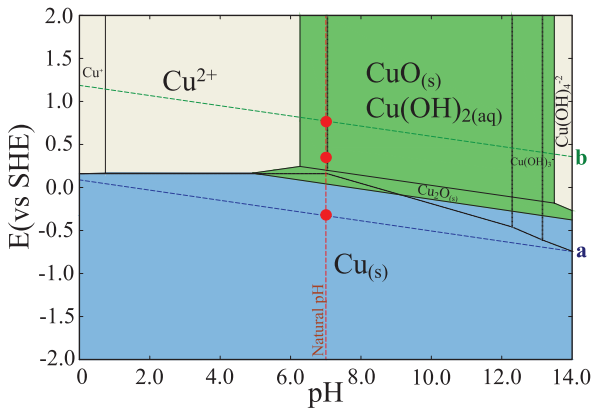

Figure 5. Calculated potential-pH (Pourbaix) diagram for copper in deaerated deionized water. The titrants were assumed to be NaOH and HNO_3. The marked points correspond to the natural condition for copper deaerated with N_2 (upper) and N_2 followed by saturation by H_2 (lower). The diagrams were generated by CorrosionAnalyzer 2.0 (Build 2.0.16) by OLI Systems Inc.

hydrogen when the water is saturated with H_2 at 1 atm pressure. This falls within the stability region for copper. For aerated electrolyte, the redox potential for water lies on the equilibrium line b for oxygen, the upper filled circle at pH = 7, where copper is not stable. For deaerated water in the absence of hydrogen, the redox potential, shown by the middle marked circle in Figure 5, lies between the lines a and b.

The redox potential is not the corrosion potential; but, it may be used as an indicator for the stability of copper. When hydrogen is present, the system may be considered to be at equilibrium, and copper is indicated to be stable. In the absence of hydrogen, the hydrogen evolution reaction may take place until sufficient hydrogen is formed to stabilize the copper. The thermodynamic simulations support the interpretation that the impedance and voltammetry results show corrosion of copper when deaerated with N_2 and that corrosion is suppressed by saturation with H_2. These results are consistent with the experimental observations reported by Hultquist[27] and with the thermodynamic analysis reported by Macdonald and Sharifi-Asl.[25]

Kinetic simulation.— Kinetic simulations were performed to explore the manner in which copper may react in deaerated water. In the absence of oxygen, the reactions were assumed to include dissolution of copper

$$Cu \rightarrow Cu^{2+} + 2e^- \quad [2]$$

and hydrogen reduction at the cathode

$$2H^+ + 2e^- \rightarrow H_2 \quad [3]$$

As the concentration of corrosion product increases, the cathodic reaction

$$Cu^{2+} + 2e^- \rightarrow Cu \quad [4]$$

begins to play a role. Generation of hydrogen may be expected to result in hydrogen oxidation

$$H_2 \rightarrow 2H^+ + 2e^- \quad [5]$$

The corresponding rate expressions were used to construct a time dependent model for the system.

A simulation was performed using the kinetic expressions for reactions 2, 3 and 4.[19] At short times, the hydrogen oxidation current is extremely low and could be ignored. At open circuit potential the net current is equal to zero; thus,

$$i_{a,Cu} + i_{c,Cu} + i_{c,H_2} = 0 \quad [6]$$

The anodic current density for copper dissolution is given by

$$i_{a,Cu} = i_{0,Cu} e^{b_{a,Cu}(V - V_{0,Cu})} \quad [7]$$

where $V_{0,Cu}$ is the equilibrium potential for the copper reaction. The corresponding cathodic current density can be expressed as

$$i_{c,Cu} = -i_{0,Cu} \left(\frac{c_{Cu^{2+}}(0)}{c_{Cu^{2+},ref}} \right)^{\gamma} e^{-b_{c,Cu}(V - V_{0,Cu})} \quad [8]$$

where the concentration term accounts for the concentration of cupric ion at the electrode surface, $c_{Cu^{2+},ref}$ is the concentration at which the exchange current density was obtained, and γ was assigned a value of 0.75. The cathodic hydrogen evolution reaction was expressed as

$$i_{c,H_2} = -i_{0,H_2} e^{-b_{c,H_2}(V - V_{0,H_2})} \quad [9]$$

where V_{0,H_2} is the equilibrium potential for the hydrogen evolution reaction. The concentration of copper at the electrode surface was assumed to be controlled by spherical diffusion from the electrode,[38] thus,

$$(i_{a,Cu} + i_{c,Cu}) = \frac{4nFD_{Cu^{2+}} r_0}{A} (c_{Cu^{2+}}(0) - c_{Cu^{2+}}(\infty)) \quad [10]$$

The three cases shown in Table II were considered. Case (I) corresponds to an initial condition in which copper dissolution is balanced by hydrogen evolution. For Case (II), accumulation of copper ions at

Table II. Summary of the time dependent reactions considered for modeling Cu corrosion kinetics.

Reaction Number	**Case I:** At Time = 0 No O_2	**Case II:** For Time > 0 No O_2	**Case III:** For Time > 0 No O_2 and H_2 Enriched
(2)	$Cu \rightarrow Cu^{2+} + 2e^-$	$Cu \rightarrow Cu^{2+} + 2e^-$	$Cu \rightarrow Cu^{2+} + 2e^-$
(3)	$2H^+ + 2e^- \rightarrow H_2$	$2H^+ + 2e^- \rightarrow H_2$	$2H^+ + 2e^- \rightarrow H_2$
(4)		$Cu^{2+} + 2e^- \rightarrow Cu$	$Cu^{2+} + 2e^- \rightarrow Cu$
(5)			$H_2 \rightarrow 2H^+ + 2e^-$

the electrode surface allows copper dissolution and reduction reactions to occur in tandem with the reduction of hydrogen. Case (III) accounts for oxidation of dissolved H_2.

The set of equations was solved simultaneously under a pseudo-steady-state approximation in which the concentration $c_{Cu^{2+}}(\infty)$ was increased incrementally by a material balance. The kinetic parameters used for the simulations are presented in Table III. As parameters from pure water were not found in the literature, data were taken for environments associated with similar reaction mechanisms. Formation of CuCl was not expected in the present system; therefore, parameters for the copper dissolution and deposition were taken from a reference reporting experiments in a sulfate electrolyte. The exchange current density used in our simulations was adjusted for the cupric ion concentration at which the exchange current was measured, as shown in equation (8). Buffered borate electrolytes have been used as a surrogate for water associated with nuclear repositories.[28,30] The parameters for the hydrogen evolution reaction at 20°C were taken from Sharifi-Asla and Macdonald, who reported results in a boric acid electrolyte with pH adjusted by addition of NaOH.[30] The resulting calculated corrosion rates, averaged over a one year period, are a strong function of pH. For the system under investigation, under the assumption that hydrogen was removed by deaeration, the corrosion rate for parameter set A obtained at a pH of 5.72 was calculated to be 7.9 nm/day. The average corrosion rate for parameters obtained at a pH of 8 (sets B, D, E, F) was calculated to be 1 nm/day. The calculated corrosion rate for hydrogen parameters obtained at a pH of 9.2 was 0.45 nm/day. In the presence of a saturated pressure of hydrogen, the net rate of corrosion (not shown in Table III) was calculated to be equal to zero. These results are in agreement with the thermodynamic results presented in Figure 5. An understanding of the results presented in Table III may be obtained from the

Table III. Kinetic parameters used for the simulation and results. Values for the equilibrium potential for the copper dissolution reaction were taken from Figure 1 of reference 39 and adjusted to be referenced to the Normal Hydrogen Electrode. The electrolyte pH for the hydrogen reaction reported in reference 30 was obtained by adding NaOH. Corrosion rates represent calculated values averaged over a one-year period.

Reaction rxn (2)[a]	pH	p_{H_2}, atm	E_0, V(NHE) -0.1876	i_0, A/cm^2 9×10^{-4}	b_a, V^{-1} 20	b_c, V^{-1} 53.56	i_{corr}, nm/day
rxn (3)[b]							
A	5.72	1	−0.331	3.46×10^{-7}	–	23.03	7.94
B	8	1	−0.465	6.76×10^{-7}	–	23.50	1.12
C	9.2	1	−0.535	1.01×10^{-6}	–	23.03	0.45
D	8	0.5	−0.456	5.43×10^{-7}	–	23.03	1.16
E	8	0.3	−0.450	4.73×10^{-7}	–	24.24	1.05
F	8	0.1	−0.436	3.28×10^{-7}	–	24.24	1.02

[a]The electrolyte was 0.7 M $CuSO_4$ in 1.5 M H_2SO_4. Data taken from reference 39.
[b]NaOH was titrated to achieved desired pH in 0.03 H_3BO_3. The electrolyte temperature was 20°C. Data taken from reference 30.

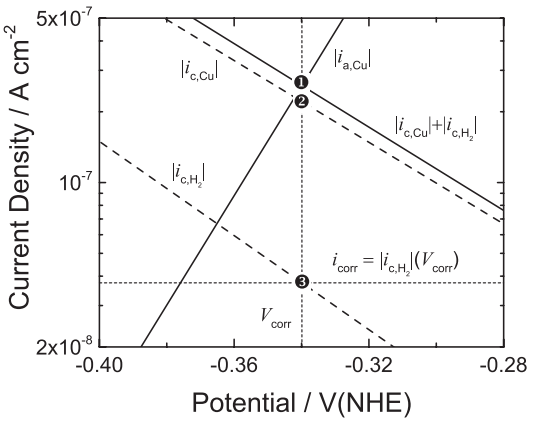

Figure 6. Evans diagram showing simulation results at $t = 0$ for hydrogen evolution, copper dissolution, and copper electrodeposition reactions corresponding to parameter set D in Table III. The solid lines correspond to the total cathodic current, $i_{c,Cu} + i_{c,H_2}$, and the anodic current $i_{a,Cu}$. The dashed lines represent the contributions of $i_{c,Cu}$ and i_{c,H_2}. The vertical line at the intersection of total cathodic and anodic current (point 1) represents the corrosion potential. The cathodic copper deposition current density at the corrosion potential is seen at point 2. The cathodic hydrogen evolution current density is seen at point 3. The corrosion current density, obtained from the difference between the copper dissolution current density at point 1 and the copper deposition current density at point 2, is equal in magnitude to the cathodic hydrogen evolution reaction at the corrosion potential (point 3).

Evan's diagram presented in Figure 6 that was taken from the simulation D at $t = 0$, for which $c_{Cu^{2+}}(\infty) = 0$. The solid lines correspond to the total cathodic current, $i_{c,Cu} + i_{c,H_2}$, and the anodic current $i_{a,Cu}$. The dashed lines represent the contributions of $i_{c,Cu}$ and i_{c,H_2}. The vertical line at the intersection of total cathodic and anodic current (point 1 in Figure 6) yields the corrosion potential $V_{corr} = -0.3399$ V. At the corrosion potential, $i_{a,Cu} = 2.582 \times 10^{-7}$ A/cm^2 and the sum of cathodic current densities has the value $i_{c,Cu} + i_{c,H_2} = -2.582 \times 10^{-7}$ A/cm^2. The cathodic copper deposition current density, seen at point 2, has the value $i_{c,H_2} = -2.208 \times 10^{-7}$ A/cm^2. The cathodic hydrogen evolution current density, seen at point 3, has the value $i_{c,H_2} = -3.745 \times 10^{-8}$ A/cm^2. The corrosion current density obtained from the sum of copper dissolution and deposition current densities is $i_{corr} = 3.745 \times 10^{-8}$ A/cm^2, corresponding to 1.2 nm/day. The calculated concentration at the electrode surface was $c_{Cu^{2+}}(0) = 2.646 \times 10^{-10}$ mol/cm^3.

The anodic copper dissolution reaction is balanced at the corrosion potential V_{corr} by the sum of hydrogen evolution and copper deposition reactions. The back deposition of copper occurs due to the accumulation of copper ions at the electrode surface. The copper dissolution and deposition reactions were not equal in magnitude because, as shown by equation (10), some of the copper ions diffuse away from the surface. In the usual application of Evan's diagrams, the cathodic reaction does not involve metal deposition and the corrosion current would be found from the intersection of the metal dissolution current and the cathodic current. In the present case, the cathodic current contains a dominant contribution from the reverse reaction to metal dissolution. Thus, the corrosion current density is obtained from the difference, measured at the corrosion potential, between the copper dissolution current density and the magnitude of the copper deposition current density. The corrosion current is equal in magnitude to the cathodic hydrogen evolution reaction at the corrosion potential.

The oxidation of hydrogen formed by the cathodic hydrogen evolution reaction was not found to be significant, and inclusion of this reaction did not change the results presented in Figure 6. Once the hydrogen partial pressure is sufficient, the corrosion rate was found to be equal to zero. These results are in agreement with the observations of Macdonald and Sharifi-Asl.[25]

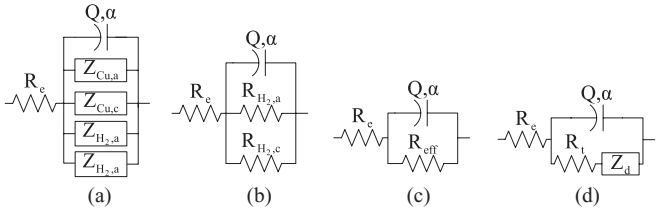

Figure 7. Equivalent electrical circuit models for the impedance data presented in Figure 3: a) general model showing the parallel contributions of all potential reactions; b) reduced model corresponding to the impedance data for gold and platinum electrodes; c) model corresponding to the impedance data for gold and platinum electrodes in terms of an effective resistance; d) model for the copper electrode.

Impedance regression analysis.— An impedance model for the data presented in Figure 7(a) should account for parallel contributions of the impedances associated with the charging current and the other reactions occurring for this system. An electrical circuit that provides a framework for such a model is presented could be expressed as Figure 7(a).

For the gold and platinum electrodes, the feasible reactions are hydrogen evolution and oxidation of the hydrogen thus produced. The circuit of Figure 7(a) is therefore reduced to Figure 7(b), where charge-transfer resistances were used to describe the electrochemical reactions. As the two resistances in parallel cannot be distinguished, the circuit of Figure 7(b) must be expressed as Figure 7(c) where

$$R_{\text{eff}} = \frac{R_{\text{H}_2,\text{a}} R_{\text{H}_2,\text{c}}}{R_{\text{H}_2,\text{a}} + R_{\text{H}_2,\text{c}}} \qquad [11]$$

The impedance is expressed as

$$Z_{\text{Au}} = R_{\text{e}} + \frac{R_{\text{eff}}}{1 + (2\pi \text{j} f)^{\alpha} \, Q R_{\text{eff}}} \qquad [12]$$

and the fitting results are presented as lines in Figure 7(a). The resulting parameters are provided in Table IV.

Several models were considered for the copper electrode. The circuit that provided the best representation of the experimental data is presented in Figure 7(d), i.e.,

$$Z_{\text{Cu}} = R_{\text{e}} + \frac{R_{\text{t}} + 1/k_{\text{W}}\sqrt{2\pi \text{j} f}}{1 + (2\pi \text{j} f)^{\alpha} \, Q \left(R_{\text{t}} + 1/k_{\text{W}}\sqrt{2\pi \text{j} f}\right)} \qquad [13]$$

The fitting results are presented as lines in Figure 7(a), and the resulting parameters are provided in Table IV. This model suggests that the impedance associated with the corrosion and hydrogen evolution reactions were too large to contribute to the impedance response. The diffusion contribution presented in the model given as Figure 7(d) may be attributed to the deposition of copper, as shown in Figure 6. This hypothesis is supported by Bojinov et al.,[29] who observed back deposition of copper. As the measured frequency range was insufficient to allow determination of the diffusion time constant, the diffusing species could not be identified. At the zero-frequency limit, the polarization resistance is related to the corrosion density, i_{corr}, using the

Table IV. Regression results for the data presented in Figure 7(a).

Parameter	Au	Pt	Cu
R_{e}, kΩcm^2	5.85 ± 0.07	4.93 ± 0.05	9.6 ± 0.5
Q, μF/s$^{(1-\alpha)}$cm^2	27.6 ± 0.3	27.6 ± 0.3	9.6 ± 0.2
α, dimensionless	0.66 ± 0.01	0.69 ± 0.01	0.73 ± 0.02
R_{eff}, kΩcm^2	790 ± 210	750 ± 170	–
R_{t}, kΩcm^2	–	–	95 ± 12
k_{W}, μS s$^{1/2}$/cm^2	–	–	24 ± 0.2
C_{eff}, μF/cm^2	10.9	11.2	3.9

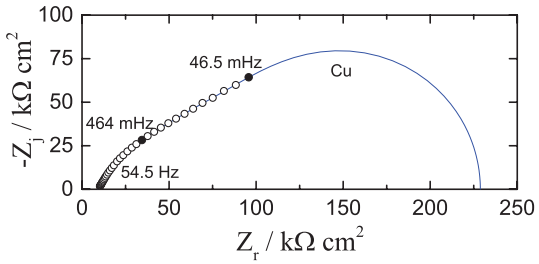

Figure 8. Measurement model extrapolation (blue line) of the copper impedance (circle) showing the predicted zero frequency limit.

Stern-Geary equation,[40]

$$i_{\text{corr}} = \frac{-\beta_{\text{H}_2}\beta_{\text{Cu}}}{2.303 R_{\text{p}} \left(\beta_{\text{Cu}} - \beta_{\text{H}_2}\right)} \qquad [14]$$

where β_{H_2} and β_{Cu} are the Tafel slope parameters obtained from literature.[30,39] As zero-frequency limit cannot be readily discerned from the impedance data, the regression results cannot provide an estimate for the corrosion rate. An estimation of an upper bound to the corrosion rate may, however, be provided. A measurement model[41,42] extrapolation of the data is presented in Figure 8. The estimation of the polarization resistance obtained from the measurement model for copper suggests that the corrosion rate must be smaller than 2.5 nm/day.

Three approaches were used to assign a physical meaning to the CPE parameters obtained by regression. As the absence of passivation behavior in the polarization curve shown in Figure 4 suggests the absence of oxide films, the Brug formula[43]

$$C_{\text{eff}} = Q^{1/\alpha} R_{\text{e}}^{(1-\alpha)/\alpha} \qquad [15]$$

was used to estimate the capacitance associated with the CPE parameters Q and α. The use of the Brug formula is further supported by analysis of the geometry-induced nonuniform current and potential distributions expected for the electrode. Huang et al.[44] showed for a disk electrode that, above a dimensionless frequency

$$K = Q(2\pi f)^{\alpha} r_0 \rho = 1 \qquad [16]$$

nonuniform current and potential distributions influence the impedance response. The resulting impedance was described as a pseudo-CPE that was best modeled by the Brug formula.[45] The dimensionless frequency K is written in equation (16) as a function of the CPE coefficient Q, the angular frequency $2\pi f$ raised to the power of the CPE exponent α, the disk radius r_0, and the electrolyte resistivity ρ. For the present system, the characteristic frequency obtained from equation (16) was 1.6 Hz, meaning that above this frequency, the impedance was influenced by a surface distribution of ohmic resistance.

The values obtained for gold and platinum electrodes, shown in Table IV, are in good agreement with expected values for electrodes in deionized water. The capacitance obtained for copper was, however, smaller than expected for an electrode-electrolyte interface. A different set of calculations were performed to explore the hypothesis that the capacitance should be associated with an oxide film. If the CPE behavior is caused by the axially-distributed properties of an oxide film, the power-law model[46,47] provides the best method to associate CPE parameters to film properties.[48] Under the assumption that the film is Cu_2O (with a dielectric constant of 7.6)[49] and that the lower limit of the film resistivity is 1000 Ωcm, the film thickness would be on the order of 190 nm. Under the assumption that the film is CuO, with a dielectric constant of 18.1,[49] the film thickness would be on the order of 350 nm. As oxide films on copper are not expected to be thicker than 6 nm,[50] the interpretation based on the Brug formula seems most appropriate.

A third approach is to attribute the capacitance obtained from the Brug equation to a film. The film thickness so obtained would range

Table V. Estimated values for copper corrosion rates.

Method	i_{corr}, mA/cm^2	i_{corr}, nm/day
Measurement model extrapolation of impedance	$<7.9 \times 10^{-5}$	<2.5
Kinetic Simulations	3.2×10^{-5}	1.1

from 1.7 for Cu_2O to 4.1 nm for CuO, which is within the range of expected values for an oxide on copper. If an oxide film is present, the polarization curve indicates that it is not protective.

Discussion

Several methods were employed in the present work to quantify the rate of copper corrosion in deaerated deionized water. The impedance analysis showed that the copper electrode behaved in a manner that was strikingly different from the gold and platinum electrodes. Thus, the impedance results suggest that the electrochemistry of copper must play a role. As the gold and platinum results were almost identical, the impedance response for these two materials should not be associated with the respective electrochemistry. The impedance data, therefore, support the hypothesis that corrosion of copper takes place in deaerated deionized water. An extrapolation of the impedance diagram to the zero-frequency limit suggests that the corrosion rate must be less than 2.5 nm/day (see Table V).

The polarization curves presented in Figure 4 provided additional verification for the electrochemical activity of copper, but changes in the electrolyte during the experiment precluded accurate assessment of a corrosion current density. As shown in Table V, the kinetic simulations suggest a corrosion rate of 1 nm/day, where kinetic parameters were obtained from electrolytes that may be considered surrogates for deionized water. The hypothesis that copper corrodes in deaerated deionized water is further supported by the Pourbaix diagram calculated for the environment under investigation. In the present work, copper was shown to be thermodynamically unstable in deaerated deionized water; whereas, thermodynamic stability was predicted for copper in deaerated deionized water equilibrated with hydrogen gas at a pressure of 1 atm. A slight increase in the concentration of dissolved hydrogen at the electrode surface is suggested by the impedance response for the inert gold and platinum electrodes, but this was apparently not sufficient to stabilize the copper.

The impedance measurements did not provide an estimate of the corrosion rate, but yielded instead an upper bound of 2.5 nm/day. The impedance results may also be used to support the claim that the deaeration procedure employed in the present work yielded very low levels of dissolved oxygen on the order of 1 ppb. If oxygen were present in the experimental system, the concentration associated with the upper bound of 2.5 nm/day would have been 6.5 ppb. The dissolved oxygen concentration in the experimental system reported here was therefore less than 6.5 ppb and, likely, based on Henry's law arguments, substantially less. The oxygen concentration yielding a corrosion rate of 1 nm/day, equal to that predicted in the absence of oxygen, would be 2.5 ppb. The corrosion rate in water containing dissolved oxygen concentrations much lower than 2.5 ppb would still be 1 nm/day, so long as hydrogen is absent. Thus, the present work shows that, in the absence of hydrogen, copper will corrode on the order of 1 nm/day in deionized water with an O_2 concentration on the order of, or less than, 1 ppb.

The corrosion rates in the present work (under anaerobic conditions) are comparable in magnitude to the corrosion rate of the copper (at 15+ ppb O_2) cooling system used at the Argonne National Laboratory synchrotron.[31,32] Here we demonstrate that a detectable copper corrosion rate (under anaerobic conditions) still occurs and does so to a measurable degree. The present work also supports the claim that copper in deaerated deionized water will corrode if hydrogen is removed from the electrolyte, as was previously observed by Hultquist[27] and discussed as a theoretical possibility by Macdonald and Sharifi-Asl.[25] The estimated corrosion rate is sufficiently small that it can be neglected for most technological applications. This rate, however, may be sufficient to cause failure of copper nanostructures employed in heat exchangers for liquid-cooling of high-performance electronics.

Conclusions

A combination of impedance and polarization experiments and thermodynamic, kinetic, and impedance models were used to assess the tendency of copper to corrode in deaerated deionized water that did not contain hydrogen. The present work shows that copper will corrode at a very small rate. Kinetic simulations indicate that, for the present experimental conditions, the average rate would be on the order of 1 nm/day. The impedance analysis suggests that the corrosion rate is less than 2.5 nm/day. This corrosion rate will decrease as the concentration of hydrogen and copper increases. While the estimated corrosion rate may be inconsequential for most technological applications, the corrosion rate is large enough to influence the functionality of copper nanostructures utilized in emerging applications.

Acknowledgments

The authors gratefully acknowledge the support of DARPA, Dr. Bar-Cohen, program manager.

References

1. A. Bar-Cohen and P. Wang, *J. Heat Transfer*, **134**, 051017 (2012).
2. S. V. Garimella and C. Sobhan, *Advances in Heat Transfer*, **35**, 249 (2001).
3. S. P. Gurrum, S. K. Suman, Y. K. Joshi, and A. G. Fedorov, *Device and Materials Reliability, IEEE Transactions on*, **4**, 709 (2004).
4. M. Groll, M. Schneider, V. Sartre, M. Chaker Zaghdoudi, and M. Lallemand, *Revue générale de thermique*, **37**, 323 (1998).
5. C. Zhang, *Analytical and Experimental Investigation of Capillary Forces Induced by Nanopillars for Thermal Management Applications*, Ph.D. dissertation, University of Texas (2010).
6. R. Chen, M.-C. Lu, V. Srinivasan, Z. Wang, H. H. Cho, and A. Majumdar, *Nano Lett.*, **9**, 548 (2009).
7. A. S. Kousalya, J. A. Weibel, S. V. Garimella, and T. S. Fisher, *Int. J. Heat Mass Tran.*, **59**, 372 (2013).
8. D. B. Tuckerman and R. Pease, *Electron Device Letters, IEEE*, **2**, 126 (1981).
9. R. W. Knight, D. Hall, J. Goodling, and R. Jaeger, *Components, Hybrids, and Manufacturing Technology, IEEE Transactions on*, **15**, 832 (1992).
10. M. Bowers and I. Mudawar, *Int. J. Heat Mass Tran.*, **37**, 321 (1994).
11. R. Chein and G. Huang, *Appl Therm Eng*, **25**, 3104 (2005).
12. S. P. Jang and S. U. Choi, *Appl Therm Eng*, **26**, 2457 (2006).
13. C.-J. Ho, L. Wei, and Z. Li, *Appl Therm Eng*, **30**, 96 (2010).
14. Y. S. Ju, M. Kaviany, Y. Nam, S. Sharratt, G. Hwang, I. Catton, E. Fleming, and P. Dussinger, *International Journal of Heat and Mass Transfer*, **60**, 163 (2013).
15. J. P. McHale, S. V. Garimella, T. S. Fisher, and G. A. Powell, *Nanoscale and Microscale Thermophysical Engineering*, **15**, 133 (2011).
16. M. Braun and K. Nobe, *J. Electrochem. Soc.*, **126**, 1666 (1979).
17. O. E. Barcia, O. R. Mattos, N. Pébère, and B. Tribollet, *J. Electrochem. Soc.*, **140**, 2825 (1993).
18. A. L. Bacarella and J. J. C. Griess, *J. Electrochem. Soc.*, **120**, 459 (1973).
19. J. S. Newman and K. E. Thomas-Alyea, *Electrochemical Systems*, 3rd edition (Hoboken, NJ: John Wiley & Sons, 2004).
20. G. Hultquist, G. Chuah, and K. Tan, *Corros. Sci.*, **29**, 1371 (1989).
21. G. Hultquist, M. Graham, P. Szakalos, G. Sproule, A. Rosengren, and L. Gråsjö, *Corros. Sci.*, **53**, 310 (2011).
22. G. Hultquist, P. Szakalos, M. Graham, A. B. Belonoshko, G. Sproule, L. Gråsjö, P. Dorogokupets, B. Danilov, T. AAstrup, and G. Wikmark et al., *Catal. Lett.*, **132**, 311 (2009).
23. F. King and C. Lilja, *Corros. Eng., Sci. Technol.*, **46**, 153 (2011).
24. P. Szakalos, G. Hultquist, and G. Wikmark, *Electrochem. Solid-State Lett.*, **10**, C63 (2007).
25. D. D. Macdonald and S. Sharifi-Asl, *Is Copper Immune to Corrosion When in Contact with Water and Aqueous Solutions*, Technical Report TR-01-23, Swedish Radiation Safety Authority, Swedish Nuclear Fuel and Waste Management Co Box 5864 SE-102 40 Stockholm Sweden (2011).
26. F. King, L. Ahonen, C. Taxen, U. Vuorinen, and L. Werme, *Copper corrosion under expected conditions in a deep geologic repository*, Technical Report TR-01-23, Swedish Nuclear Fueland Waste Management Co, Swedish Nuclear Fuel and Waste Management Co, Box 5864, SE-102 40 Stockholm Sweden (2001).
27. G. Hultquist, P. S. I. Szakálos, M. J. Graham, G. I. KingSproule, and G. Wikmark, "Detection of Hydrogen in Corrosion of Copper in Pure Water," in *Proceedings of the 2008 International Corrosion Congress*, Paper 3884 (2008) 1–9.

28. M. Bojinov, I. Betova, and C. Lilja, *Corros. Sci.*, **52**, 2917 (2010).
29. M. Bojinov, T. Laitinen, K. Mäkelä, M. Snellman, and L. Werme, *MRS Proceedings*, **807**, 459 (2003).
30. S. Sharifi-Asla and D. D. Macdonald, *J. Electrochem. Soc.*, **160**, H382 (2013).
31. R. Dortwegt and E. Maughan, "The Chemistry of Copper in Water and Related Studies Planned at the Advanced Photon Source," in *Proceedings of the Particle Accelerator Conference, PAC 2001*, volume 2 (IEEE, 2001) 1456–1458.
32. R. Dortwegt, C. Putnam, and E. Swetin, "Mitigation of Copper Corrosion and Agglomeration in APS Process Water Systems," in *2nd Intl Workshop on Mechanical Engineering Design of Synchrotron Radiation Equipment and Instrumentation (MEDSI2002)* (2002) 462–468.
33. M. Parro, P. Karditsas, A. Caloutsis, D. Iglesias, B. Brañas, and A. Abánades, "Corrosion and Activation Analysis of the LIPAC Beam Dump Cooling Circuit," *Fusion Eng. Des.*, **86**, 827–830 (2013).
34. J. S. Newman, *J. Electrochem. Soc.*, **113**, 501 (1966).
35. A. Anderko and P. J. Shuler, *Computers & Geosciences*, **23**, 647 (1997).
36. A. Anderko, S. J. Sanders, and R. D. Young, *Corrosion*, **53**, 43 (1997).
37. B. Beverskog and I. Puigdomenech, *J. Electrochem. Soc.*, **144**, 3476 (1997).
38. P. Mahon and K. Oldham, *Anal. Chem.*, **77**, 6100 (2005).
39. Z. Stanković and M. Vuković, *Electrochim. Acta*, **41**, 2529 (1996).
40. M. Stern and A. L. Geary, *J. Electrochem. Soc.*, **104**, 56 (1957).
41. P. Agarwal, M. E. Orazem, and L. H. García-Rubio, *J. Electrochem. Soc.*, **139**, 1917 (1992).
42. M. E. Orazem, P. T. Wojcik, M. Durbha, I. Frateur, and L. H. García-Rubio, "Application of Measurement Models for Interpretation of Impedance Spectra for Corrosion," *Materials Science Forum*, **289–292**, 813 (1998).
43. G. J. Brug, A. L. G. van den Eeden, M. Sluyters-Rehbach, and J. H. Sluyters, *J. Electroanal. Chem.*, **176**, 275 (1984).
44. V. M.-W. Huang, V. Vivier, I. Frateur, M. E. Orazem, and B. Tribollet, *J. Electrochem. Soc.*, **154**, C89 (2007).
45. B. Hirschorn, M. E. Orazem, B. Tribollet, V. Vivier, I. Frateur, and M. Musiani, *Electrochim. Acta*, **55**, 6218 (2010).
46. B. Hirschorn, M. E. Orazem, B. Tribollet, V. Vivier, I. Frateur, and M. Musiani, *J. Electrochem. Soc.*, **157**, C452 (2010).
47. B. Hirschorn, M. E. Orazem, B. Tribollet, V. Vivier, I. Frateur, and M. Musiani, *J. Electrochem. Soc.*, **157**, C458 (2010).
48. M. E. Orazem, B. Tribollet, V. Vivier, S. Marcelin, N. Pébère, A. L. Bunge, E. A. White, D. P. Riemer, I. Frateur, and M. Musiani, *J. Electrochem. Soc.*, **160**, C215 (2013).
49. W. M. Haynes, T. J. Bruno, and D. R. Lide, editors, *CRC Handbook of Chemistry and Physics*, 94th edition (CRC Press, 2014).
50. R. Bogdanowicz, J. Ryl, K. Darowicki, and B. B. Kosmowski, *J. Solid State Electrochem.*, **13**, 1639 (2009).